Examining the spatial and temporal variability of evaporative demand across the conterminous United States

Michael Hobbins[1], David Streubel[2], Andrew Wood[1], and Kevin Werner[1]

[1]Colorado Basin River Forecast Center/NWS/NOAA, Salt Lake City, UT 84116; [2]Hydrology and Climate Services Division, Western Region NWS/NOAA, Salt Lake City, UT 84103
mike.hobbins@noaa.gov, dave.streubel@noaa.gov, andy.wood@noaa.gov, kevin.werner@noaa.gov

1. CENTRAL QUESTION

Assuming a physically sound formulation, what drives the spatial and temporal variability of evaporative demand (E_0) across the conterminous US?

2. ABSTRACT

Due to the essentially unknowable nature of the distribution of soil and vegetative moisture at the temporal and spatial scales useful to water managers, hydrologists have long used the concept of evaporative demand (E_0) to describe the upper limit to actual evapotranspiration (*ET*). E_0 then drives hydrologic models or empirical relations that account for soil moisture conditions and vegetative constraints on moisture transfer to estimate actual *ET*.

To improve its streamflow forecast skill, the Colorado Basin River Forecast Center (CBRFC) is replacing the current static E_0 driver of its river forecast model (a climatological monthly pan evaporation value derived from outdated data) with one that is temporally dynamic and physically sound: synthetic pan evaporation (E_{pan}) from the PenPan model [ref 1].

Given the hydroclimatologic heterogeneity and varied temporal scales of CBRFC operations, it is essential to characterize the temporal and spatial variability of the new E_0 driver, in both its magnitude and its sources. Here we examine the temporal and spatial variability in E_{pan} using a first-order, second-moment uncertainty analysis applied to a gridded reanalysis time-series of E_{pan} across various time-scales and CONUS-wide. Our results have broad implications in hydrology, but particularly for the CBRFC, can help identify which drivers require the most pre-processing in such formulations, and which, perhaps, may be ignored in moving to a forecast context that has fewer data inputs available.

3. MODELING EVAPORATIVE DEMAND

Goal: A 30-year reanalysis of E_0 using E_{pan}

Evaporative demand (E_0) has been observed as E_{pan} for many decades on a daily basis at US class-A evaporation pans around the world. The PenPan model [ref 1] synthesizes E_{pan} well [ref 2], using only meteorological drivers commonly observed at the land surface.

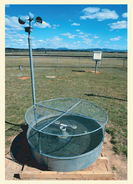

Fig 1: A typical US class-A evaporation pan.

Model formulation

The PenPan model modifies the Penman equation [ref 3] for potential evaporation to better characterize the enhanced radiative and advective dynamics of US class-A evaporation pans:

$$\lambda E_{pan} = \frac{\Delta}{\Delta + a_p\gamma} Q_n + \frac{a_p\gamma}{\Delta + a_p\gamma} f_q(U_2)(e_{sat} - e_a) \qquad (1)$$

In eqn (1), λ is the latent heat of vaporization; U_2 is the 2-m wind speed; $f_q(U_2)$ is the wind function; e_{sat} and e_a are the saturated and actual vapor pressures, respectively; Δ is de_{sat}/d_T at *T*; a_p is the ratio of effective surface areas for heat and water-vapor transfer in a pan; γ is the psychrometric constant; and Q_n is the net available energy for E_{pan}.

North American Land Data Assimilation System (NLDAS) drivers [ref 4]

- *T*, air temperature at 2 m
- *q*, specific humidity at 2 m
- R_d, downwelling shortwave radiation
- L_d, downwelling longwave radiation
- P_{atm}, station pressure
- U_{10}, wind speed at 10 m
- 1/8th-degree spatial resolution
- CONUS-wide
- Hourly time-step
- January 1, 1980, to December 31, 2009

E_{pan} was generated on a daily basis from January 1, 1980, to December 31, 2009. Shown here are the mean and variance of annual E_{pan} aggregated from daily totals; similar results may be obtained for daily to annual time-frames. As expected, and in line with E_{pan} observations [ref 5], annual E_{pan} is highest in the sunniest, warmest, driest, and windiest regions. The annual variability of E_{pan}, here estimated by its variance, does not match the spatial pattern of its annual magnitude (see fig 2).

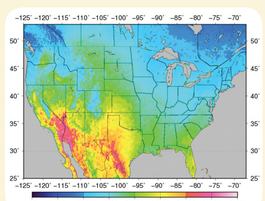

Fig 2: Mean annual E_{pan}, as estimated by the PenPan model forced by NLDAS data, 1980-2009 (mm/year).

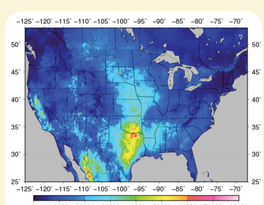

Fig 3: Variance of annual E_{pan}, as estimated by the PenPan model forced by NLDAS data, 1980-2009 (mm²/year²).

4. VARIABILITY ANALYSIS

Concept

E_{pan} is a function of its six drivers:

$$E_{pan} = f\{T, q, U_{10}, R_d, L_d, P_{atm}\} \qquad (2)$$

The variability in E_{pan} (σ^2_{Epan}) derives from the variability in all its drivers acting independently and covarying, which are composed of sensitivities, variances, and covariances:

$$\sigma^2_{E_{pan}} = f\left\{\begin{array}{l} \sigma^2_T\left(\frac{\partial E_{pan}}{\partial T}\right)^2, \sigma^2_q\left(\frac{\partial E_{pan}}{\partial q}\right)^2, \sigma^2_{U_{10}}\left(\frac{\partial E_{pan}}{\partial U_{10}}\right)^2, \\ \sigma^2_{R_d}\left(\frac{\partial E_{pan}}{\partial R_d}\right)^2, \sigma^2_{L_d}\left(\frac{\partial E_{pan}}{\partial L_d}\right)^2, \sigma^2_{P_{atm}}\left(\frac{\partial E_{pan}}{\partial P_{atm}}\right)^2, covariances \end{array}\right\} \qquad (3)$$

The full expression for the variability in E_{pan} expressed as a function of the contributions from all of its components in the first-order, second-moment uncertainty analysis framework:

$$\sigma^2_{E_{pan}} \approx \frac{\partial E_{pan}}{\partial T}^2 \sigma^2_T + \frac{\partial E_{pan}}{\partial q}^2 \sigma^2_q + \frac{\partial E_{pan}}{\partial R_d}^2 \sigma^2_{R_d} + \frac{\partial E_{pan}}{\partial L_d}^2 \sigma^2_{L_d} + \frac{\partial E_{pan}}{\partial P_{atm}}^2 \sigma^2_{P_{atm}} + \frac{\partial E_{pan}}{\partial U_{10}}^2 \sigma^2_{U_{10}}$$

contribution of individual drivers varying independently

$$+2\left(\begin{array}{l} \frac{\partial E_{pan}}{\partial T}\frac{\partial E_{pan}}{\partial q}\sigma_{T,q} + \frac{\partial E_{pan}}{\partial T}\frac{\partial E_{pan}}{\partial U_{10}}\sigma_{T,U_{10}} + \frac{\partial E_{pan}}{\partial T}\frac{\partial E_{pan}}{\partial R_d}\sigma_{T,R_d} + \frac{\partial E_{pan}}{\partial T}\frac{\partial E_{pan}}{\partial L_d}\sigma_{T,L_d} \\ + \frac{\partial E_{pan}}{\partial T}\frac{\partial E_{pan}}{\partial P_{atm}}\sigma_{T,P_{atm}} + \frac{\partial E_{pan}}{\partial q}\frac{\partial E_{pan}}{\partial U_{10}}\sigma_{q,U_{10}} + \frac{\partial E_{pan}}{\partial q}\frac{\partial E_{pan}}{\partial R_d}\sigma_{q,R_d} + \frac{\partial E_{pan}}{\partial q}\frac{\partial E_{pan}}{\partial L_d}\sigma_{q,L_d} \\ + \frac{\partial E_{pan}}{\partial q}\frac{\partial E_{pan}}{\partial P_{atm}}\sigma_{q,P_{atm}} + \frac{\partial E_{pan}}{\partial U_{10}}\frac{\partial E_{pan}}{\partial L_d}\sigma_{U_{10},L_d} + \frac{\partial E_{pan}}{\partial U_{10}}\frac{\partial E_{pan}}{\partial P_{atm}}\sigma_{U_{10},P_{atm}} + \frac{\partial E_{pan}}{\partial U_{10}}\frac{\partial E_{pan}}{\partial R_d}\sigma_{U_{10},R_d} \\ + \frac{\partial E_{pan}}{\partial R_d}\frac{\partial E_{pan}}{\partial L_d}\sigma_{R_d,L_d} + \frac{\partial E_{pan}}{\partial R_d}\frac{\partial E_{pan}}{\partial P_{atm}}\sigma_{R_d,P_{atm}} + \frac{\partial E_{pan}}{\partial L_d}\frac{\partial E_{pan}}{\partial P_{atm}}\sigma_{L_d,P_{atm}} \end{array}\right) \qquad (4)$$

contribution from interdependence of all driver pairs

Sensitivities, Variances, and Covariances

The sensitivities of E_{pan} to each of its drivers are derived analytically (eqns (6) - (10)) from the model formulation (see eqn (1)), and evaluated at drivers' mean values.

$$\frac{\partial(\lambda E_{pan})}{\partial L_d} = f_T \qquad (5)$$

$$\frac{\partial(\lambda E_{pan})}{\partial P_{atm}} = -\frac{\lambda(1-f_T)f_q(U_2)q}{0.622 + 0.378q} \qquad (6)$$

$$\frac{\partial(\lambda E_{pan})}{\partial U_{10}} = \lambda(1-f_T)1.39 * 10^{-8}(e_{sat} - e_a)1.35\left(\frac{2}{10}\right)^{\frac{1}{7}} \qquad (7)$$

$$\frac{\partial(\lambda E_{pan})}{\partial q} = -\lambda(1-f_T)f_q(U_2)P_{atm}\frac{0.622}{(0.622 + 0.378q)^2} \qquad (8)$$

$$\frac{\partial(\lambda E_{pan})}{\partial R_d} = f_T(1-\alpha_p)\frac{R_d 1.31(P_{rad} - 1.42)}{R_{tot}} + \frac{R_n}{R_d} \qquad (9)$$

$$\frac{\partial(\lambda E_{pan})}{\partial T} = f_T\left((1-\alpha_p)\frac{R_d^2 1.31(P_{rad} - 1.42)}{R_{tot}}\frac{2361}{\lambda} - 4\sigma\varepsilon T^3\right) + 0.0115(R_n + L_d - \sigma\varepsilon T^4) + \lambda(1-f_T)f_q(U_2)e_{sat}\frac{4098.171}{(T - 35.85)^2} + f_q(U_2)(e_{sat} - e_a)(54.303T - 30648.8834) \qquad (10)$$

Fig 5 shows an example of sensitivity: of E_{pan} to U_{10}. As expected from eqn (1), the sensitivity of E_{pan} to U_{10} is greatest in areas where the vapor pressure deficit (i.e., $e_{sat} - e_a$) is the greatest. The converse is presumably also true: the sensitivity of E_{pan} to vapor pressure deficit is greatest in the windiest areas (not shown).

Figs 4 and 6 shows examples of the spatial patterns of variance (of U_{10}) and covariance (of U_{10} and R_d), respectively. As might be expected, the variance of U_{10} is greatest along the coasts, the Great Lakes and in the higher elevations of the western US and Appalachians. It is difficult to draw meaningful conclusions regarding the covariance of U_{10} and R_d: indeed, covariances between many pairs of variables can be slight

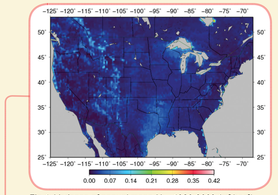

Fig 4: Variance of annual mean U_{10}, 1980-2009 (m²/sec²).

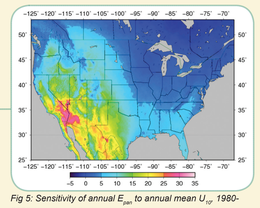

Fig 5: Sensitivity of annual E_{pan} to annual mean U_{10}, 1980-2009 ((mm/year)/(m/sec)).

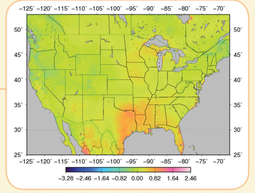

Fig 6: Covariance of annual mean U_{10} and annual mean R_d, 1980-2009 (W/m.sec).

Dominant Drivers of Variability

The drivers contributing the greatest variability to E_{pan} vary significantly across different time-frames. Annually (top), a coastal/continental distinction emerges, with *T* dominating E_{pan} variability across the heart of the continent and R_d across the Northeast, the Southeast, and the Pacific Northwest. Undifferentiated covarying pairs of drivers dominate across the rest of CONUS. In winter (center), when E_{pan} is at its lowest, *T* becomes the dominant variability driver of monthly E_{pan}. In the vital summer months (bottom), R_d dominates across the eastern half of CONUS, while the undifferentiated covarying pairs of drivers dominate the High Plains region, and *T* and U_{10} drive E_{pan} variability across western CONUS.

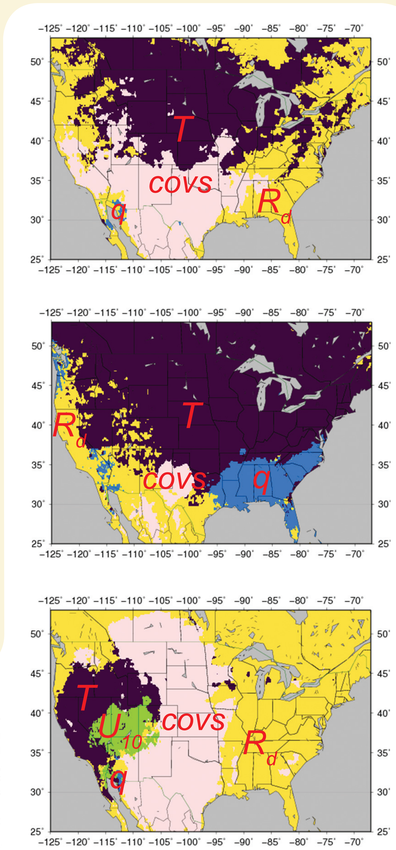

Fig 7: The dominant driver of variability in (top) annual E_{pan}; (center) monthly E_{pan} for July; and (bottom) monthly E_{pan} for January.

6. REFERENCES

1. Linacre, ET (1994), Estimating U.S. class A pan evaporation from few climate data, Water International, 19, 5–14.
2. Roderick, ML, LD Rotstayn, GD Farquhar, and MT Hobbins (2007), On the attribution of changing pan evaporation, Geophys. Res. Lett., 34, L17403.
3. Penman, HL (1948), Natural evaporation from open water, bare soil, and grass. Proc. Royal Soc., London, vol. A, 193, 120–145.
4. The NLDAS data used in this study are acquired as part of the mission of NASA's Earth Science Division and archived and distributed by the Goddard Earth Sciences (GES) Data and Information Services Center (DISC).
5. Farnsworth, RK, ES Thompson, and EL Peck (1982), Evaporation atlas for the contiguous 48 United States, NOAA Technical Report NWS 33, 27 pp., US Dept of Commerce, Washington, D.C..
6. Thornthwaite, CW (1948), An approach toward a rational classification of climate. Geog. Rev., 38, 55–94.
7. Hamon, WR (1961), Estimating potential evapotranspiration, J. Hyd. Div., ASCE. 87(HY3),107-120.
8. Hargreaves, GH and ZA Samani (1985), Reference crop evapotranspiration from temperature, Appl. Eng. in Ag., 1, 96–99.
9. Palmer, WC (1965), Meteorological drought, Res. Pap. 45, 58 pp., US Dept of Commerce, Washington, D.C..
10. Dai, A, T Trenberth, and KE Qian (2004), A global dataset of Palmer Drought Severity Index for 1870– 2002: Relationship with soil moisture and effects of surface warming, J. Hydromet., 5, 117–130.
11. Robock, A, M Mu, K Vinnikov, IV Trofimova, and TI Adamenko (2005), Forty-five years of observed soil moisture in the Ukraine: No summer desiccation (yet), Geophys. Res. Lett., 32, L03401.
12. Hobbins, MT, A Dai, ML Roderick, and GD Farquhar (2008), Revisiting the parameterization of potential evaporation as a driver of long-term water balance trends, Geophys. Res. Lett., 35, L12403.

5. CONCLUSIONS

Toward the goal of understanding the predictability of the energy and water cycles, a rigorous first-order, second-moment variability analysis of synthetic E_{pan}, a physically sound measure of E_0, demonstrates the contributions to E_0-variability by all of its drivers varying alone or covarying in pairs. For annual E_{pan}, we indicate where each driver dominates and we hint at the implications of seasonal variability.

Correctly identifying and including the dominant drivers of E_0 variability is crucial for any hydrologic application that estimates actual *ET* from models driven by E_0, such as streamflow forecasting and drought analyses. Due to their simplicity, E_0 parameterizations based solely on *T* [refs 6, 7, 8] are used in areas and applications for which they are ill-suited, as in the use of the Palmer Drought Severity Index (PDSI) [ref 9] in the US Drought Monitor for tracking ongoing droughts and the analysis of secular drought trends. Using the *T*-based E_0 parameterization in the standard PDSI has led to predictions of long-term mid-latitude continental drying [ref 10], in contrast to observations [ref 11]. When forced by E_{pan} observations, the PDSI estimates both drying and wetting [ref 12], in line with observations.

As we show here, across most of CONUS, not only is *T* not the greatest driver of annual E_0 variability, but where it does dominate, such dominance wanes in the important months of the growing season. Across nearly all coastal regions, R_d contributes the greatest variability in annual E_{pan}. In many other parts of the country for much of the year no single driver dominates E_{pan}, and instead covarying drivers must be considered.

This analysis is predicated on the central assumption that E_{pan} from the PenPan model synthesizes E_0 well, an assumption that locks in this suite of drivers. To ensure that we are not begging the question, a principal components analysis of observations of E_{pan} with respect to the same suite of drivers will indicate the soundness of this assumption.

Most results shown here are for annual E_{pan} aggregated from daily modeling. Similar analyses are possible at all time-frames down to the daily scale. Seasonal analyses will focus on evaporative demand during the all-important growing and water supply seasons.